

Computational Design of Skintight Clothing

JUAN MONTES, Concordia University

BERNHARD THOMASZEWSKI, Université de Montréal & ETH Zürich

SUDHIR MUDUR, Concordia University

TIBERIU POPA, Concordia University



Fig. 1. Our method automatically generates patterns for skintight clothing, considering design objectives related to shape, comfort, and function. In this example, a set of initial patterns (*left*) is optimized such as to reduce the traction forces acting on the seams, yielding complex patterns (*right*) that lead to aesthetically pleasing results (*middle, right*).

We propose an optimization-driven approach for automated, physics-based pattern design for tight-fitting clothing. Designing such clothing poses particular challenges since large nonlinear deformations, tight contact between cloth and body, and body deformations have to be accounted for. To address these challenges, we develop a computational model based on an embedding of the two-dimensional cloth mesh in the surface of the three-dimensional body mesh. Our *Lagrangian-on-Lagrangian* approach eliminates contact handling while coupling cloth and body. Building on this model, we develop a physics-driven optimization method based on sensitivity analysis that automatically computes optimal patterns according to design objectives encoding body shape, pressure distribution, seam traction, and other criteria. We demonstrate our approach by generating personalized patterns for various body shapes and a diverse set of garments with complex pattern layouts.

CCS Concepts: • **Computing methodologies** → **Physical simulation**; • **Applied computing** → **Computer-aided manufacturing**.

Additional Key Words and Phrases: computational design, pattern optimization, physically-based modelling, seam design

Authors' addresses: Juan Montes, Concordia University, juans.montes@gmail.com; Bernhard Thomaszewski, Université de Montréal & ETH Zürich, bernhard@iro.umontreal.ca; Sudhir Mudur, Concordia University, mudur@cs.concordia.ca; Tiberiu Popa, Concordia University, tiberiu.popa@concordia.ca.

Permission to make digital or hard copies of all or part of this work for personal or classroom use is granted without fee provided that copies are not made or distributed for profit or commercial advantage and that copies bear this notice and the full citation on the first page. Copyrights for components of this work owned by others than ACM must be honored. Abstracting with credit is permitted. To copy otherwise, or republish, to post on servers or to redistribute to lists, requires prior specific permission and/or a fee. Request permissions from permissions@acm.org.

© 2020 Association for Computing Machinery.

0730-0301/2020/7-ART105 \$15.00

<https://doi.org/10.1145/3386569.3392477>

ACM Reference Format:

Juan Montes, Bernhard Thomaszewski, Sudhir Mudur, and Tiberiu Popa. 2020. Computational Design of Skintight Clothing. *ACM Trans. Graph.* 39, 4, Article 105 (July 2020), 12 pages. <https://doi.org/10.1145/3386569.3392477>

1 INTRODUCTION

Whether as casual clothing, functional sportswear, or medical compression garments—skintight clothing has many applications, and *fit* is of central importance to all of them. The fit of a garment is determined by its design which, from a technical perspective, consists of two components: (1) a layout that determines the number of patterns and how they connect to each other and (2) the shape of the individual patterns. When fitting a design to a given body shape, the layout is typically kept fix, whereas the pattern shapes are adjusted in order to accommodate different body shapes and sizes. This task of *pattern grading* is a challenging problem, since the designer has to simultaneously consider multiple criteria that relate to the state of the garment once worn.

Although shape is largely determined by the underlying body, there is often substantial room for shape control within the limits of comfort and physics. The shape and location of the seams on the body is another design consideration, important for both aesthetic and functional goals. Apart from these visual criteria, there are several objectives relating to the deformations induced in clothing and body. For example, excessive tensile deformations will affect comfort and may cause fabric and seams to deteriorate prematurely. Compressions, on the other hand, induce wrinkles that are typically perceived as design flaws in tight-fitting clothing. Designing pattern shapes that strike an ideal balance between these criteria requires time and expertise, both of which are important cost factors.

In this work, we present an automated, optimization-driven fitting approach for skintight clothing. As the technical core of our method,

we propose a unified simulation model that represents cloth as a two-dimensional elastic membrane embedded in the surface of the deformable body mesh. This *Lagrangian-on-Lagrangian* approach removes the need for detecting and handling collisions between body and cloth. Our approach supports continuous tangential motion (i.e., sliding) of cloth on smooth body meshes during simulation and optimization, allowing us to take advantage of efficient continuous optimization methods. We introduce a set of design objectives that model various design goals related to shape, comfort, and function. In particular, our method allows for minimizing traction forces on the seams, for enforcing lower and upper bounds on deformations to prevent wrinkles and material failure, for controlling pressure forces exerted on the body, and for modeling body shapes and contours.

We demonstrate our method on a set of designs that are representative of different use cases for skintight clothing. We show examples from casual clothing, personalized sportswear, and patient-specific compression garments.

2 RELATED WORK

Designing skintight clothing is a multidisciplinary problem that spans several subfields in visual computing and engineering. We structure our survey of related work into shape decomposition and parameterization, coupling between deformable systems, general garment modeling, and tight-fitting clothing design.

Shape Decomposition & Parameterization. Decomposing a 3D shape into 2D patches is a fundamental problem in graphics, relevant to a large number of practical applications. Early solutions [Julius et al. 2005; Lévy et al. 2002; Sander et al. 2001; Sorkine et al. 2002; Yamauchi et al. 2005; Zhou et al. 2004] rely on bottom-up approaches to grow quasi-developable regions until a certain developability threshold is reached. While these methods offer little control over the patch boundaries or the number of patches to be used, more recent works [Li et al. 2018b; Poranne et al. 2017] overcome these limitations through joint optimization of the seams and distortion of the parameterization.

Designing patterns for manufacturing adds additional layers of complexity to the problem. Mori et al. [2007] developed a system for making plush toys, and Skouras et al. [2014] developed a system for fabrication of inflatable structures. Sharp and Crane [2018] frame the problem of mesh decomposition as a 3D boundary optimization over a continuous domain. While each of these methods is effective for the specific application they pursue, they do not readily extend to the tightly-coupled mechanics of clothing and body that we target with our work.

Coupling Deformable Systems. A main difficulty in modeling and simulating clothing is that body and cloth are in close contact. Existing methods handle contact using impulses [Bridson et al. 2002; Harmon et al. 2008], penalty forces [Baraff and Witkin 1998; Harmon et al. 2009; Wang 2018] or constraints [Li et al. 2018a; Müller et al. 2015; Otaduy et al. 2009], and resort to geometric resolution strategies for missed collision [Baraff et al. 2003; Volino and Magnenat-Thalmann 2006]. While these models are well-suited for conventional clothing with few or intermittent collisions, the many

high-pressure contact points inherent to skintight clothing pose substantial challenges.

An alternative approach for coupling deformable systems in contact is the so-called Eulerian-on-Lagrangian representation in which one mechanical system is embedded in (a subspace of) the other [Cirio et al. 2014, 2015; Fan et al. 2013; Li et al. 2013; Sueda et al. 2011; Weidner et al. 2018], thus eliminating the need for explicit contact handling. The *hosting* system is represented using a Lagrangian mesh, which in turn provides an Eulerian discretization for the *embedded* system. Li et al. [2013] demonstrate this approach by simulating elastic skin as a single patch in texture space. Unfortunately, this approach does not readily extend to skintight clothing, which generally requires multiple patches with nontrivial connections. Instead of using an Eulerian representation for the embedded system, another approach is to use a second Lagrangian mesh whose degrees of freedom are expressed relative to the hosting system using, e.g., barycentric coordinates. However, using a piecewise linear discretization for the hosting system (e.g., a triangle or tetrahedron mesh), leads to discontinuous derivatives when the embedded mesh slides over the hosting mesh. Zehnder et al. [2016] address this problem by using a smooth representation based on subdivision surfaces for the hosting system in order to simulate elastic curves on rigid surfaces. Our approach follows the same strategy for simulation, but treats both hosting (i.e., body) and embedding (i.e., cloth) systems as elastic materials.

Garment Modeling. Clothing design is a time- and cost-intensive process that typically requires the skill and expertise of trained professionals. Accelerating and automating this task is therefore a topic of intense research and existing methods can roughly be divided into two categories. One line of work uses interactive techniques such as sketching in order to quickly generate or edit garments [Decaudin et al. 2006; Robson et al. 2011; Turquin et al. 2007; Umetani et al. 2011; Wang et al. 2005]. The work by Umetani et al. [2011] allows designers to edit garments either in pattern or world space and uses sensitivity analysis to predict the change in equilibrium shape. Design automation methods adapt existing garments to bodies of different shapes and sizes with little or no user interaction required [Bartle et al. 2016; Brouet et al. 2012; Meng et al. 2012]. For example, Chen et al. [2015] propose a method for adapting a garment using the 3D body geometry obtained from a depth camera. The method by Berthouzoz et al. [2013] parses patterns made by professional designers, automatically identifies the salient features, and adapts them to virtual characters. Guan et al. [2012] propose a method that uses machine learning to generate garment animations for virtual characters with a wide range of body shapes. While our method falls into the latter category of design automation, the various design objectives that we introduce offer ample room for user control.

Designing Tight-fitting Clothing. Tight-fitting clothing is ubiquitous in casual fashion, functional sportswear, medical garments, and many other applications. Despite their prevalence, however, there has only been relatively little research into design tools for this type of clothing. Exceptions include the work by Kwok et al. [2016] who present a method for full-body skintight clothing design. Their focus is on finding optimal patch configurations that minimize a fitness

energy based on heuristic distortion measures. Wang et al. [2008; 2010] present methods to optimize for patterns that achieve prescribed pressure distributions. While this is also one of our goals, our computational model is more general in that it incorporates deformations of the body and allows seams to move on the body during optimization. While these capabilities require higher technical complexity and sophistication, they allow us to define additional design objectives for controlling the body shape and fabric stretch as well as to minimize seam traction and garment sliding during motion.

3 COMPUTATIONAL MODEL

Our method for optimization-driven pattern design of skintight clothing builds on a dedicated computational model that we present in this section. We start by describing our representation that provides intrinsic coupling between cloth and body (Sec. 3.1). Based on this representation, we introduce strain energies for the different materials (Sec. 3.2) and describe the formulation and solution of the forward simulation problem (Sec. 3.3).

3.1 Lagrangian-on-Lagrangian Representation

The interaction between cloth and body must be modeled in a way that will allow us to capture the relevant physical phenomena with sufficient accuracy and efficiency. A conceptually straightforward approach is to model garment and body using independent discretizations that are coupled through contact forces [Wang 2018]. For the case of skintight clothing, however, where all parts of the garment are in tight contact with the body, handling coupling through penalty forces would lead to high computational costs. We therefore take a different route that we refer to as a *Lagrangian-On-Lagrangian* approach: while the body is discretized into a tetrahedral mesh, we represent the garment as an embedded triangle mesh whose vertices are expressed relative to the surface of the 3D body mesh. By embedding the garment mesh in the surface of the body mesh, we eliminate the need for collision detection and contact handling while achieving accurate mechanical coupling between the two systems, including sliding and pressure forces.

We represent the body as a tetrahedral mesh with $\mathbf{y} = (\mathbf{y}_1, \dots, \mathbf{y}_m) \in \mathbb{R}^{3n}$ and $\bar{\mathbf{y}} = (\bar{\mathbf{y}}_1, \dots, \bar{\mathbf{y}}_m) \in \mathbb{R}^{3n}$, denoting vertex positions in its deformed and undeformed configuration, respectively. The rest state of the garment is defined by collection of 2D mesh patches whose vertices we denote by $\bar{\mathbf{x}}_i \in \mathbb{R}^2$. We assume that the connectivity between the patches, i.e. which patch boundaries are to be stitched together, is known. For the deformed configuration of the garment, let $\mathbf{s} = (\mathbf{s}_1, \dots, \mathbf{s}_n)$ denote the vertex positions relative to the deformed body mesh \mathbf{y} . More concretely, $\mathbf{s}_i = (tri_i, u_i, v_i)$ holds the index tri_i of the body mesh triangle containing \mathbf{s}_i and corresponding local coordinates (u_i, v_i) . Using this embedded approach, the vertex positions $\mathbf{x} = (\mathbf{x}_1, \dots, \mathbf{x}_n) \in \mathbb{R}^3$ of the garment in its deformed configuration become a function of the corresponding relative positions \mathbf{s} and the deformed body mesh \mathbf{y} , i.e., $\mathbf{x}_i = \mathbf{x}_i(\mathbf{s}_i, \mathbf{y})$. One way to define this function is through piece-wise linear interpolation, in which case \mathbf{s}_i are simply barycentric coordinates and \mathbf{x}_i become convex combinations of the corresponding triangle vertices \mathbf{y}_j . While conceptually simple, a central drawback of this approach

is the fact that, since \mathbf{x} is linear on each triangle, its derivatives are discontinuous across triangles. This discontinuity is already a severe problem for simulation, and it makes optimization grind to a halt in suboptimal configurations.

To achieve sufficient smoothness without introducing additional variables or constraints, we follow the approach by Zehnder et al. [2016] and turn to subdivision surfaces. More concretely, we use Loop subdivision and define $\mathbf{x}_i(\mathbf{s}_i, \mathbf{y})$ as the positions on the corresponding limit surface, which is C_2 -continuous everywhere except near irregular vertices and whose derivatives can be evaluated at arbitrary locations [Stam 1998]. The additional smoothness greatly benefits both simulation and optimization, but since Loop subdivision is not interpolatory, there is a slight discrepancy between cloth and body surfaces. However, since this difference quickly diminishes with increasing mesh resolution, we consider this approach an acceptable compromise.

3.2 Material Modeling

To arrive at the system of equations that govern static equilibrium configurations of the cloth-body system, we must first define how deformations relate to strain energy and how to discretize the corresponding quantities.

Body. We use linear tetrahedron finite elements to discretize the body. To define the strain energy for a given tetrahedron element, we first introduce the finite-element interpolation for its deformed and undeformed geometry as

$$\mathbf{y}(\mathbf{u}) = \sum_i^4 N_i(\mathbf{u})\mathbf{y}_i \quad \text{and} \quad \bar{\mathbf{y}}(\mathbf{u}) = \sum_i^4 N_i(\mathbf{u})\bar{\mathbf{y}}_i, \quad (1)$$

where $\mathbf{u} \in \Omega_e \subset \mathbb{R}^3$ are rest state coordinates from the undeformed element's parametric domain Ω_e and $N_i : \Omega_e \rightarrow \mathbb{R}$ are the four linear basis functions uniquely defined through $N_i(\bar{\mathbf{y}}_j) = \delta_{ij}$. The deformation of the element is described by its deformation gradient \mathbf{F}_B and the corresponding right Cauchy-Green tensor \mathbf{C}_B , which are defined as

$$\mathbf{F}_B = \frac{\partial \mathbf{y}}{\partial \bar{\mathbf{y}}} \quad \text{and} \quad \mathbf{C}_B = \mathbf{F}_B^T \mathbf{F}_B, \quad (2)$$

respectively. We model the body as a Neo-Hookean solid (see, e.g., [Bonet and Wood 2008]), whose energy density function is defined as

$$W_{\text{body}}(\mathbf{C}) = \frac{\mu}{2}(\bar{I}_1(\mathbf{C}) - 3) + \frac{\lambda}{2}(J(\mathbf{C}) - 1)^2, \quad (3)$$

where $J = \det \mathbf{C}_B^{1/2}$ and $\bar{I}_1 = J^{-2/3} \mathbf{C}_B$. To obtain the elastic energy per element, we integrate (3) over the tetrahedron's undeformed domain. Since the basis functions are linear, the deformation gradient and consequently the energy density are constant over the element. The total strain energy therefore follows as

$$U_{\text{body}} = \sum_e U_{\text{body}}^e = \sum_e V^e W_{\text{body}}(\mathbf{C}_B^e), \quad (4)$$

where V^e is per-element volume in the undeformed configuration.

Cloth. Since the mechanics of the cloth are dominated by in-plane deformation, we use linear triangle finite elements, so called Constant Strain Triangles, for discretization. Although skintight clothing is mostly stretched, there are typically regions in which elements experience compression. Unlike their response to stretching, fabrics oppose very little resistance to compression and instead wrinkle immediately. Modeling this behavior in a finite element setting is challenging, as standard material models exhibit equal resistance to stretching and compression at the origin. We therefore turn to tension field theory [Pipkin 1986] to define a relaxed strain energy that does not penalize compression while offering sufficient smoothness for simulation and optimization. We largely follow Skouras et al. [2014] but instead of using a rubber-like material model, we use the St.Venant-Kirchhoff model (StVK) which is better suited for fabric simulation [Volino et al. 2009]. In analogy to the volumetric setting described above, we start with the finite-element interpolation for deformed and undeformed geometry,

$$\mathbf{x}(\mathbf{v}) = \sum_i^3 N_i(\mathbf{v})\mathbf{x}_i \quad \text{and} \quad \bar{\mathbf{x}}(\mathbf{v}) = \sum_i^3 N_i(\mathbf{v})\bar{\mathbf{x}}_i, \quad (5)$$

where $\mathbf{v} \in \Omega_C \subset \mathbb{R}^2$ are rest state coordinates parameterized over the undeformed triangle's domain Ω_C and $N_i : \Omega_C \rightarrow \mathbb{R}$ are its three linear basis functions. We likewise introduce the deformation gradient \mathbf{F}_C and the corresponding right Cauchy-Green tensor \mathbf{C}_C ,

$$\mathbf{F}_C = \frac{\partial \mathbf{x}}{\partial \bar{\mathbf{x}}} \quad \text{and} \quad \mathbf{C}_C = \mathbf{F}_C^T \mathbf{F}_C. \quad (6)$$

It is worth noting that, since $\mathbf{x} \in \mathbb{R}^3$ and $\bar{\mathbf{x}} \in \mathbb{R}^2$, the deformation gradient \mathbf{F}_C is a 3×2 -matrix and \mathbf{C}_C is 2×2 -matrix describing the deformation of the CST element with respect to rest state coordinates. Its eigenvalues $\lambda_1 \geq \lambda_2$ represent the maximum and minimum stretch squared. Finally, after introducing the 2D Green-Lagrange strain as $\mathbf{E}_C = \frac{1}{2}(\mathbf{C}_C - \mathbf{I}_2)$ with \mathbf{I}_2 the 2×2 identity matrix, we can define the StVK strain energy density function as

$$W_{\text{StVK}} = \frac{\lambda}{2} \text{tr}(\mathbf{E}^2) + \mu \text{tr}(\mathbf{E}^2), \quad (7)$$

where λ and μ are the Lamé material parameters. To arrive at a relaxed form of the StVK energy that does not penalize compressions, we define three energy regimes whose activation depends on the element's principal stretches, i.e., the eigenvalues of \mathbf{C}_C . If $\lambda_2 \leq \lambda_1 < 1.0$, the element is *slack* and its energy vanishes. If the minimum stretch λ_2 is less than its energetic minimum $\bar{\lambda}_2(\lambda_1) = \text{argmin}_{\lambda_2} W_{\text{StVK}}$ while the maximum stretch $\lambda_1 > 1.0$, the element is *wrinkled* and the energy has to be modified such that the stress in the direction of minimum stretch vanishes. If $\lambda_1 \geq 1$ and $\lambda_2 \geq \bar{\lambda}_2(\lambda_1)$, the element is *taut* and the regular StVK energy is used. To implement these changes, we rewrite the StVK energy in terms of principal stretches as

$$W_{\text{StVK}} = \frac{\lambda}{8} (\lambda_1 + \lambda_2 - 2)^2 + \frac{\mu}{4} [(\lambda_1 - 1)^2 + (\lambda_2 - 1)^2]. \quad (8)$$

Noting that the energetic minimum for λ_2 is

$$\bar{\lambda}_2(\lambda_1) = \text{argmin}_{\lambda_2} W_{\text{StVK}}(\lambda_1) = \frac{2\lambda + 2\mu - \lambda\lambda_1}{\lambda + 2\mu}, \quad (9)$$

we define the relaxed energy model for StVK as

$$W_{\text{cloth}}(\lambda_1, \lambda_2) = \begin{cases} 0 & \lambda_1 < 1, \lambda_2 < 1 \\ W_{\text{StVK}}(\lambda_1, \bar{\lambda}_2(\lambda_1)) & \lambda_1 \geq 1, \lambda_2 < \bar{\lambda}_2(\lambda_1) \\ W_{\text{StVK}}(\lambda_1, \lambda_2) & \text{otherwise} \end{cases} \quad (10)$$

It should be noted that this energy density function is only C_1 -continuous with respect to the principal stretches. Since our optimization algorithm requires continuous second derivatives of the energy, we smooth the discontinuous transitions in the forces using quadratic interpolation [Skouras et al. 2014]. Since the deformation gradient and the energy density are constant for each triangle element, the strain energy for the cloth follows in analogy to the solid case as

$$U_{\text{cloth}} = \sum_e U_{\text{cloth}}^e = \sum_e t A^e W_{\text{cloth}}(\lambda_1^e, \lambda_2^e), \quad (11)$$

where A^e is the per-triangle area in the undeformed configuration and t the thickness of the fabric.

Seams. When sewing patterns together to create the garment, the seams will generally exhibit a stiffer response to stretching than the base fabric: seams involve at least two layers of fabric and the yarn and the compaction that they create further increases stiffness. The precise material properties depend on the type of seam and yarn material and can be determined experimentally [Pabst et al. 2008]. Our model incorporates seam stiffening through tensile elements that are added to the boundary of the patches. To this end, we introduce an additional energy for each seam edge

$$U_{\text{seam}} = \frac{1}{2} w t \frac{E}{l_0} (l - l_0)^2, \quad (12)$$

where E is the Young's modulus of the seam, w and t are its width and depth respectively, and l and l_0 denote the deformed and undeformed length of the seam edge.

3.3 Simulation

With all individual energies defined, the total potential energy of the coupled cloth-body system follows as

$$U = U_{\text{cloth}}(\mathbf{x}(\mathbf{s}, \mathbf{y})) + U_{\text{seam}}(\mathbf{x}(\mathbf{s}, \mathbf{y})) + U_{\text{body}}(\mathbf{y}). \quad (13)$$

In order for this system to be in equilibrium, the derivative of (13) must vanish with respect to the degrees of freedom describing the deformed configuration, i.e.,

$$\mathbf{f}_s(\mathbf{s}) = \frac{\partial U_{\text{cloth}}}{\partial \mathbf{s}} + \frac{\partial U_{\text{seam}}}{\partial \mathbf{s}} = \mathbf{0}, \quad (14)$$

$$\mathbf{f}_y(\mathbf{y}) = \frac{\partial U_{\text{body}}}{\partial \mathbf{y}} + \frac{\partial U_{\text{cloth}}}{\partial \mathbf{y}} + \frac{\partial U_{\text{seam}}}{\partial \mathbf{y}} = \mathbf{0}, \quad (15)$$

where \mathbf{f}_y are net body forces, and \mathbf{f}_s are generalized forces acting on the degrees of freedom for the cloth. To simplify notation, we rewrite the equilibrium conditions as

$$\mathbf{g}(\mathbf{q}) = (\mathbf{f}_s(\mathbf{s}), \mathbf{f}_y(\mathbf{y})) = \mathbf{0}, \quad \mathbf{q} = (\mathbf{s}, \mathbf{y}) \quad (16)$$

where \mathbf{q} denotes the vector holding all degrees of freedom of the coupled system. We compute equilibrium configurations by solving

Eq. (16) using Newton’s method. Each iteration requires the solution of a linear system of the form

$$\frac{\partial^2 U}{\partial \mathbf{q}^2} \Delta \mathbf{q} = -\frac{\partial U}{\partial \mathbf{q}}. \quad (17)$$

The matrix of this system—i.e., the Hessian of the total energy—may become indefinite during simulation, in which case we add exponentially increasing diagonal regularization until it can be factorized with Cholesky decomposition.

Subdivision Representation and Vertex Migration. The limit geometry of the subdivision surface for a given triangle k is determined through the one-ring of surrounding vertices as

$$\mathbf{x}(u, v) = \sum_{i=1}^K L_i^K(u, v) \mathbf{y}_{i(k)}, \quad (18)$$

where L_i^K are the Loop subdivision basis functions and $\mathbf{y}_{i(k)}$ selects the corresponding body vertices for the patch. It should be noted that the derivatives of the cloth energy in Eq. (14) and (15),

$$\frac{\partial U_{\text{cloth}}}{\partial \mathbf{s}} = \frac{\partial U_{\text{cloth}}}{\partial \mathbf{x}} \frac{\partial \mathbf{x}}{\partial \mathbf{s}} \quad \text{and} \quad \frac{\partial U_{\text{cloth}}}{\partial \mathbf{y}} = \frac{\partial U_{\text{cloth}}}{\partial \mathbf{x}} \frac{\partial \mathbf{x}}{\partial \mathbf{y}}, \quad (19)$$

require the Jacobian of (18) with respect to local coordinates \mathbf{s} as well as the derivatives with respect to the vertices \mathbf{y} . Likewise, computing the Hessian in (17) requires the second derivatives of (18). For regular vertices ($K = 12$), the Loop basis functions and their derivatives can be computed analytically. For irregular vertices, we use the numerical evaluation scheme due to Stam [1998].

As the cloth slides over the body during simulation, vertices may migrate from one triangle to another. The subdivision representation ensures that these transitions are almost always C_2 -continuous and at worst C_1 -continuous near irregular vertices. Nevertheless, since the local coordinate systems of neighboring triangles are generally different, we have to update the search direction such that

$$\frac{\partial \mathbf{x}_n}{\partial \mathbf{s}} \Delta \mathbf{s}_n = \frac{\partial \mathbf{x}_o}{\partial \mathbf{s}} \Delta \mathbf{s}_o, \quad (20)$$

where the indices o and n refer to the old and new triangle, respectively.

4 OPTIMIZATION

Based on the forward simulation model introduced in the previous section, we build an optimization-driven pattern design algorithm that we describe next. We start by stating the design problem in its generic form as

$$\min T(\mathbf{x}(\mathbf{q}), \mathbf{p}) \quad \text{s.t.} \quad \mathbf{g}(\mathbf{q}) = \mathbf{0}, \quad (21)$$

where $\mathbf{q} = (\mathbf{s}, \mathbf{y})$ as before, $\mathbf{g}(\mathbf{q})$ are equilibrium constraints given through (16), T is a combination of design objectives and regularizers, and \mathbf{p} are design parameters controlling the shape of the cloth patterns. Instead of modeling the equilibrium constraints explicitly using Lagrange multipliers, we use sensitivity analysis to arrive at a reduced-dimensional, unconstrained minimization problem in which only the design parameters appear as variables.

Sensitivity Analysis. For every admissible choice of design parameters \mathbf{p} , there exists a locally-unique equilibrium configuration \mathbf{q} such that \mathbf{q} is effectively a function of \mathbf{p} , i.e., $\mathbf{q} = \mathbf{q}(\mathbf{p})$. The map between \mathbf{p} and \mathbf{q} is given implicitly through the equilibrium constraints $\mathbf{g}(\mathbf{q}, \mathbf{p}) = \mathbf{0}$, whose explicit dependence on \mathbf{p} is due to the cloth forces \mathbf{f}_s depending on the pattern shapes; see Eq. (16). Around a given equilibrium pair (\mathbf{q}, \mathbf{p}) , any change to the design parameters will entail corresponding changes to the configuration such that the system is again in equilibrium, which implies that

$$\frac{d\mathbf{g}}{d\mathbf{q}} = \frac{\partial \mathbf{g}}{\partial \mathbf{p}} + \frac{\partial \mathbf{g}}{\partial \mathbf{q}} \frac{\partial \mathbf{q}}{\partial \mathbf{p}} = \mathbf{0}. \quad (22)$$

Using this observation, we can express the objective gradient as

$$\frac{dT}{d\mathbf{p}} = \frac{\partial T}{\partial \mathbf{p}} + \frac{\partial \mathbf{q}^T}{\partial \mathbf{p}} \frac{\partial T}{\partial \mathbf{q}} = \frac{\partial T}{\partial \mathbf{p}} - \frac{\partial \mathbf{g}^T}{\partial \mathbf{p}} \frac{\partial \mathbf{g}^{-1}}{\partial \mathbf{q}} \frac{\partial T}{\partial \mathbf{q}}, \quad (23)$$

We note that this way of computing the objective gradient—also known as adjoint sensitivity analysis—requires the solution of a linear system whose matrix is the same as for the forward problem (17). For faster convergence, we use this gradient in combination with L-BFGS [Nocedal and Wright 2006] and line search for robustness. Besides the linear solve, each iteration of L-BFGS requires the solution of one or several forward problems to compute the equilibrium configuration for updated parameters.

Pattern Parametrization. The shapes of the cloth patterns are defined completely through their boundaries, which in turn are controlled by the design parameters \mathbf{p} . Nevertheless, evaluating elastic energies and their derivatives requires triangle meshes and we must therefore determine the position of interior vertices as a function of the boundary shape. For this purpose, we use bi-harmonic coordinates [Wang et al. 2015] and express the location of the pattern mesh vertices $\bar{\mathbf{x}}$ as a linear function of the design parameters \mathbf{p} given by the matrix \mathbf{W} of bi-harmonic weights, $\bar{\mathbf{x}} = \mathbf{W}\mathbf{p}$.

Under extreme deformations of the path boundary, the optimizer may fail to find a next iteration were the elements are well-shaped. When this happens, we resample the boundary and isotropically remesh the patches.

4.1 Regularizers

In addition to the design goals that we describe in Sec. 5, the objective function T in Eq. (21) also includes several regularizers that ensure well-shaped patterns and manufacturability.

Seam Compatibility. Connecting two patches in a given seam requires the corresponding patch boundaries to have the same length. To enforce this compatibility condition during optimization, we penalize length deviations for corresponding edges \mathbf{e}_{left} and $\mathbf{e}_{\text{right}}$ from different sides of the seam have as

$$R_{\text{SeamLen}} = \sum_i \left[\left(\|\mathbf{e}_{\text{left}}^i\|_2 - \|\mathbf{e}_{\text{right}}^i\|_2 \right)^2 \right]. \quad (24)$$

Patch Boundary. We generally prefer patch boundaries that are smooth and, excepting corners, discourage sharp features with a penalty term based on the discrete bending energy from [Bergou

et al. 2008] as

$$R_{\text{Smooth}} = \sum_{(i,j) \in \mathcal{B}} \frac{\kappa_{ij}^2}{\|\mathbf{e}_i\| + \|\mathbf{e}_j\|},$$

where \mathcal{B} is the set of pairs of consecutive edges on the pattern boundary with integrated curvature

$$\kappa_{ij} = \frac{2\mathbf{e}_i \perp \mathbf{e}_j}{\|\mathbf{e}_i\| \|\mathbf{e}_j\| + \mathbf{e}_i \cdot \mathbf{e}_j}.$$

To prevent too close approach between neighboring boundary vertices, we furthermore use the energy defined in Eq. (24) to penalize differences in length between two consecutive edges.

Patch Compactness. To prevent patterns from becoming arbitrarily thin during optimization, we introduce a compactness term that penalizes small ratios of Euclidean and on-boundary distance between two boundary vertices. Since for any pair of boundary vertices there are two possible on-boundary paths, we choose the initially shortest one and keep it for the remainder of the optimization. For two given boundary vertices $\mathbf{p}_i, \mathbf{p}_j$ we compute this ratio as

$$\rho_{ij} = \frac{\|\mathbf{p}_i - \mathbf{p}_j\|_2}{\sum_{k=i+1}^{k=j} \|\mathbf{p}_k - \mathbf{p}_{k-1}\|_2}, \quad (25)$$

where \mathbf{p}_k represent vertices in the path from \mathbf{p}_i to \mathbf{p}_j . The corresponding penalty term is defined as $R_{\text{Comp}} = \sum_i \sum_j R_{\text{Comp}}^{ij}$ where

$$R_{\text{Comp}}^{ij} = \begin{cases} (\rho_{ij} - r_D)^4 & \rho_{ij} \leq r_D \\ 0 & \rho_{ij} > r_D \end{cases} \quad (26)$$

where r_D is a threshold modeling the minimum admissible ratio.

Forces on Boundary. When designing skintight clothing, it is often desirable to prescribe the location of the garment boundaries relative to the body. Examples include the top of the waistband for a pair of pants, or the boundaries of a wet-suit close to the knee. To implement these constraints, we fix vertices on the boundary of the garment to corresponding target locations on the body. However, doing so can lead to large tangential forces on the garment boundary. We therefore encourage traction-free boundaries through the penalty term

$$R_{\text{Fixed}} = \sum_{i \in \mathcal{F}} \|\mathbf{b}_i\|_2^2 \quad \text{where} \quad \mathbf{b}_i = \frac{dU}{ds_i}, \quad (27)$$

and \mathcal{F} is the index set of fixed boundary vertices.

5 DESIGN OBJECTIVES

Our optimization-driven pattern design framework is completed by a set of design objectives that can be combined according to the requirements of a given application. We first introduce the individual objectives, then provide examples in Sec. 6.

5.1 Shape Objective

Within the limits set by physics and comfort, skintight clothing often provides room for shaping the underlying body. Our coupled model allows us to exploit this ability in our automated pattern

design framework. For this purpose, we introduce a shape objective that measures the distance between the current deformed cloth and a given target shape. For better shape approximation, we avoid restrictive per-vertex correspondence and instead use a distance-field approach based on implicit moving least squares (IMLS) surfaces [Öztireli et al. 2009]. The corresponding objective is defined as

$$T_{\text{shape}} = \sum_i \sum_k \left(\frac{\sum_k \mathbf{n}_k \cdot (\mathbf{x}_i - \mathbf{c}_k) \phi(\|\mathbf{x}_i - \mathbf{c}_k\|)}{\phi(\|\mathbf{x}_i - \mathbf{c}_k\|)} \right)^2, \quad (28)$$

where \mathbf{c}_k are the vertices of the target shape and ϕ is a locally supported kernel function,

$$\phi(r) = \left(1 - \frac{r^2}{h^2} \right)^4, \quad (29)$$

that vanishes beyond the cut-off distance h .

5.2 Stretch & Compression Objective

The amount of stretch that a garment experiences once worn is an important design consideration for skintight clothing. For instance, a tight fit can improve aerodynamic efficiency by reducing wind resistance in applications such as cycling. Then again, excessive stretch can cause material fatigue and reduce the lifetime of a garment. We therefore introduce an objective that allows designers to impose target values for minimum and maximum stretch. To this end, we first define a per-element objective as

$$T_{\text{stretch}}^e(\lambda_i^e) = \begin{cases} A^e(\lambda_i^e - \lambda_{\min})^2 & \lambda_i^e < \lambda_{\min} \\ A^e(\lambda_i^e - \lambda_{\max})^2 & \lambda_i^e > \lambda_{\max} \\ 0 & \lambda_{\min} < \lambda_i^e < \lambda_{\max} \end{cases}, \quad (30)$$

where are λ_i^e with $i = \{1, 2\}$ are the eigenvalues of the element's right Cauchy-Green tensor \mathbf{C}_C (6), $\lambda_{\min} \leq \lambda_i^e \leq \lambda_{\max}$ is the range of admissible stretch and A^e is the area of the undeformed element. The total objective simply sums up all per-element contributions as

$$T_{\text{stretch}} = \sum_e \sum_{i \in \{1,2\}} [T_{\text{stretch}}^e(\lambda_i^e)].$$

It should be noted that, since \mathbf{C}_C is a 2×2 matrix, its eigenvalues and their derivatives can be determined analytically.

In addition to defining the range of preferred stretch values, this objective also serves the purpose of penalizing wrinkled and slack elements. The latter are particularly troublesome as they can induce ill-conditioning in the Hessian at equilibrium, which causes problems for both simulation and optimization. To avoid these degenerate cases, we use the stretch objective for bounding the minimum stretch in all our examples.

5.3 Pressure Objective

Controlling the pressure that the fabric exerts on the body is an important feature for medical garments such as diabetic wear or post-surgery pressure masks. With these applications in mind, we introduce a design objective that allows the user to indicate a range of preferred pressure values.

Using the definition of pressure as the normal force per unit area, an intuitive discrete pressure definition is obtained as the normal

force per vertex divided by its corresponding area. While the normal force is readily computed in our model, there are many ways of defining per-vertex area and each definition will potentially lead to different pressure distributions. We experimented with several alternatives, and while many of them work well for regular meshes, we found that none of them provided satisfying pressure distributions for general meshes. Fig. 2 reveals the noisy discrete pressure distribution obtained when using Voronoi areas [Meyer et al. 2003] on an example whose analytical solution is constant pressure.

In order to avoid these discretization artefacts, we seek an alternative definition of pressure in the continuous setting. Turning to fluid mechanics, we find such a definition in the generalized Young-Laplace equation due to Wang et al. [2013], which describes the difference in pressure across a thin membrane in terms of interface curvature and stress. The generalized Young Laplace equation reads

$$p = \text{ttr}(\sigma\Lambda), \quad (31)$$

where Λ is the shape operator, σ is the Cauchy stress tensor, and t is the thickness of the cloth. We discretize this expression on a per-element basis using the discrete shape operator based on mid-edge normals by Grinspun et al. [2006]. This operator is defined as

$$\Lambda_e = \sum_{i=1,2,3} \frac{\theta_i + 2s_i\phi_i}{2A^e l_i} \mathbf{t}_i \mathbf{t}_i^T \quad (32)$$

where i enumerates the edge of a given element e , l_i are corresponding edge lengths, \mathbf{t}_i are in-plane normals to the edge vectors, $s_i \in \{-1, 1\}$, and θ_i are signed angles between the normals of the faces shared by the corresponding edge. The auxiliary variables ϕ_i , which determine the mid-edge normals, are obtained by minimizing

$$\psi = \sum_e A^e \text{tr}(\Lambda_e^2), \quad (33)$$

which is quadratic in ϕ and can therefore be minimized by solving a single linear system. We furthermore note that, for any choice of \mathbf{x} , there is a unique minimizer such that ϕ effectively becomes a function of \mathbf{x} , i.e., $\phi = \phi(\mathbf{x})$. Having determined the auxiliary variables, we can compute per-element pressures and define the pressure objective as

$$T_{\text{pressure}} = \sum_e A^e (p_e - \hat{p}_e)^2, \quad (34)$$

where \hat{p}_e are target pressure values. When evaluating the gradient for this objective with respect to the design parameters \mathbf{p} , we also have to account for the auxiliary variables $\phi = \phi(\mathbf{x})$,

$$\frac{dT_{\text{pressure}}}{d\mathbf{p}} = \frac{\partial T_{\text{pressure}}}{\partial \mathbf{p}} + \frac{\partial \mathbf{x}^T}{\partial \mathbf{p}} \left(\frac{\partial T_{\text{pressure}}}{\partial \mathbf{x}} + \frac{\partial \phi^T}{\partial \mathbf{x}} \frac{\partial T_{\text{pressure}}}{\partial \phi} \right). \quad (35)$$

Instead of evaluating the entire sensitivity matrices $\frac{\partial \mathbf{x}}{\partial \mathbf{p}}$ and $\frac{\partial \phi}{\partial \mathbf{x}}$, we use adjoint sensitivity analysis for both corresponding terms, which amounts to an additional linear solve per gradient evaluation.

Unlike the discrete pressures based on per-vertex areas, our new approach leads to accurate pressure distributions even for unstructured meshes with many irregular vertices and a wide range of element aspect ratios; see Fig. 2 for a comparison.

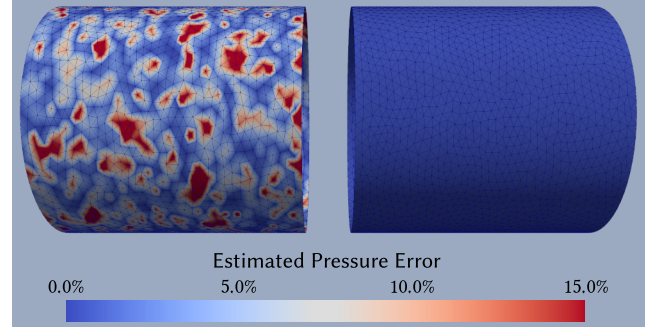


Fig. 2. Error in pressure for a piece of cloth stretched on a cylinder of radius 1.0. Left: per-vertex force divided by per-vertex Voronoi area. Right: our approach based on the Young-Laplace equation. The error is computed with respect to the analytical solution and clamped at 15%.

5.4 Seam Traction Objective

The most vulnerable areas of sewn garments are typically along the seams. It is therefore a natural goal to optimize for patterns that minimize seam stress and thus increase garment life span and reliability. For each cloth element adjacent to a seam, we evaluate the second Piola-Kirchhoff stress tensor \mathbf{S}_i [Bonet and Wood 2008], which relates traction forces to areas in the undeformed configuration, and compute the traction in the direction \mathbf{n} , perpendicular to the seam. We then penalize seam traction as

$$T_{\text{seam}} = \sum_{i \in \mathcal{T}} l_0^i t \mathbf{S}_i \mathbf{n}_i \cdot \mathbf{n}_i, \quad \text{with} \quad \mathbf{S}_i = 2 \frac{\partial W_{\text{cloth}}^i}{\partial \mathbf{C}_C}, \quad (36)$$

where \mathcal{T} is the set of all seam-adjacent elements, l_0^i is the length of the seam in the undeformed configuration, and t is the thickness of the fabric. We illustrate this optimization in Fig. 1 where a helical seam pattern yields lower stress on the seam than a straight seam pattern.

5.5 Sliding Objective for Multiple Poses

While the objectives introduced so far all refer to a single body pose, they can readily be extended to incorporate multiple poses. However, an additional aspect that arises when considering a range of motion instead of a single pose is garment sliding. Running and cycling, for instance, are applications where sustained tangential motion of the garment relative to the body can lead to discomfort and even injury.

Motivated by this example, we introduce a design objective that aims at minimizing garment sliding for a given range of motion. To this end, we start by defining a neutral body pose \mathbf{y}_0 and a set of target poses $(\mathbf{y}_1, \dots, \mathbf{y}_n)$ that represent the range of motion to be considered. We first compute the equilibrium configuration \mathbf{q}_0 for the main pose and use the resulting local coordinates \mathbf{s}_0 to determine deformed cloth positions $(\mathbf{x}_1, \dots, \mathbf{x}_n)$ for each target pose. In the absence of friction, these configurations are generally not in equilibrium and would lead to cloth sliding over the body. By accounting for friction, however, we can determine whether the unbalanced tangential forces can be compensated by friction forces.

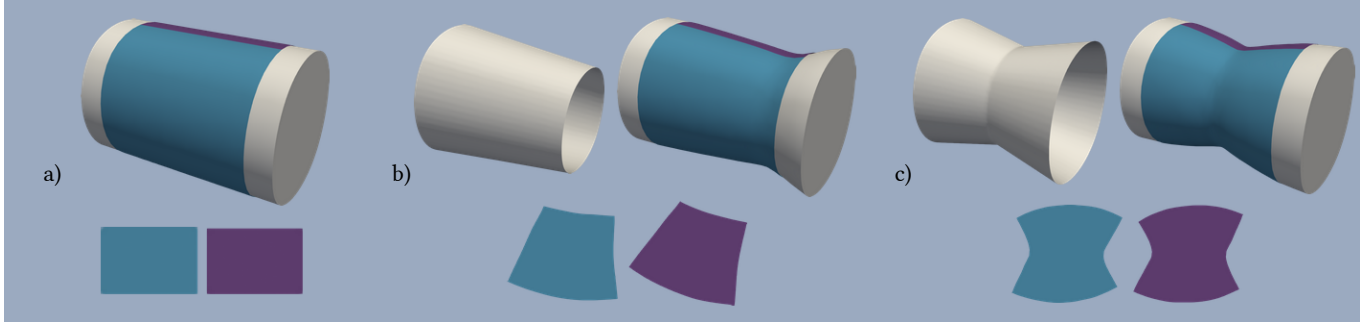


Fig. 3. Shape optimization on a cylindrical elastic body: a) initial body shape and patterns. b) Target shape of a conically tapered cylinder along with optimized patterns and corresponding simulation result. c) Target shape of an "hourglass" cylinder with optimized patterns and corresponding simulation result.

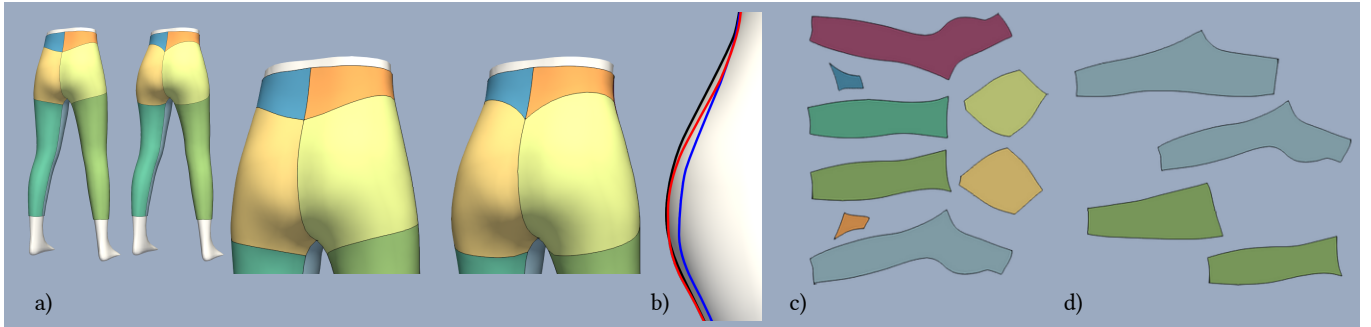


Fig. 4. Shape optimization on a virtual human: a) Shape before (left) and after (right) optimization. b) Silhouette view: initial (dark blue), optimized (red) and target (black). c) Optimized patterns. d) Two selected patterns before (top) and after optimization (bottom).

To this end, we implement a simple, isotropic Coulomb-type friction model and define tangential and friction forces magnitudes for each cloth vertex j and each pose i as

$$f_{i,j}^t = \|\mathbf{f}_{i,j} - (\mathbf{f}_{i,j} \cdot \mathbf{n}_{i,j})\mathbf{n}_{i,j}\|, \quad \text{and} \quad f_{i,j}^c = \mu \mathbf{f}_{i,j} \cdot \mathbf{n}_{i,j},$$

respectively, where $\mathbf{f}_{i,j}$ is the elastic force from the cloth, $\mathbf{n}_{i,j}$ is the normal given by the subdivision surface and μ is the friction coefficient. To penalize excessive tangential forces that would lead to sliding, we define the objective

$$T_{\text{slide}}^i = \sum_j (T_{i,j})^2, \quad T_{i,j} = \begin{cases} f_{i,j}^t - f_{i,j}^c & f_{i,j}^t \geq f_{i,j}^c \\ 0 & \text{otherwise} \end{cases}. \quad (37)$$

The gradient for this objective depends only on the local coordinates of the neutral pose and is obtained as

$$\frac{dT_{\text{slide}}}{d\mathbf{p}} = \sum_i \frac{\partial T_{\text{slide}}^i}{\partial \mathbf{p}} + \left(\frac{\partial \mathbf{x}_i}{\partial \mathbf{s}_0} \frac{\partial \mathbf{s}_0}{\partial \mathbf{p}} \right)^T \frac{\partial T_{\text{slide}}^i}{\partial \mathbf{x}_i}, \quad (38)$$

where $\frac{\partial \mathbf{s}_0}{\partial \mathbf{p}}$ is the sensitivity matrix of the neutral pose, and $\frac{\partial \mathbf{x}_i}{\partial \mathbf{s}_0}$ maps changes in local coordinates for the neutral pose to corresponding world-space changes for the target poses.

6 RESULTS AND DISCUSSION

We demonstrate our optimization-driven pattern design method on a set of examples inspired from fashion, sportswear, and medical garment applications. We start with examples that highlight

the impact of individual design objectives, then proceed to further evaluation and performance data.

6.1 Impact of Design Objectives

The design objectives can be combined arbitrarily as required by the application. All our examples use the principal stretch objective in order to discourage the formation of slack elements. However, we choose to activate only one additional objective per example in order to provide a clearer impression of their individual impact.

Shape Objective. We demonstrate our shape objective on two examples. The first one, shown in Fig. 3, uses a cylindrical shape as the initial body pose (Fig. 3a-top) and two target shapes: a conically tapered cylinder (Fig. 3b) and an hourglass shape (Fig. 3c). For both of these examples the cloth is composed of two rectangular patches (Fig. 3a-bottom) which conform to the surface of the cylinder. The optimized patterns are shown in Fig. 3b,c-bottom, and the corresponding simulation results indicate that optimizing patterns with our shape objective is an effective means of controlling body deformations. It should be noted, however, that the space of physically-feasible body deformations is fairly constrained as, e.g., volume changes cannot be achieved in this way. Nevertheless, our method is able to approximate mostly feasible target shapes with good accuracy.

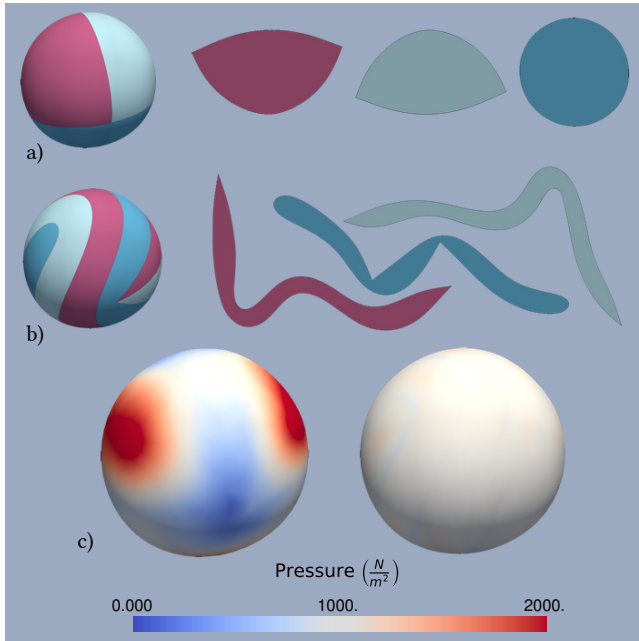


Fig. 5. Pressure objective illustrated on a sphere with a target pressure of $1000N/m^2$. a) initial and b) optimized patterns. c) pressure distributions for initial patterns (left) and optimized patterns (right).

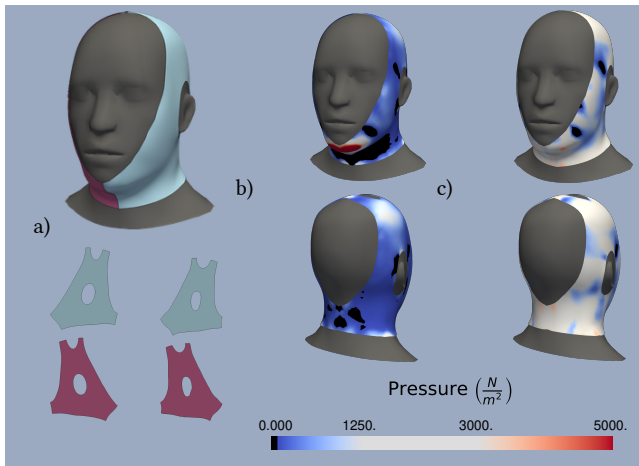


Fig. 6. Pattern optimization for a pressure mask. Areas shown in white represent pressure within the admissible range, black indicates negative pressure. a) Mask patterns, before optimization (left) and after optimization (right) b) patterns and simulation result before and c) after optimization.

The second example for the shape objective inspired by shapewear applications. Fig. 4 shows a pair of pants with its pattern atlas before and after optimization. The difference between the target shape, initial simulation result, and simulation result after optimization is shown in Fig. 4b. While the changes in geometry are perhaps less obvious than in the previous example, the changes in pattern

shape are substantial and the corresponding simulation result closely approximates the target shape.

Seam Traction Objective. To demonstrate the impact of our seam traction objective, we use it for optimizing the patterns of a pair of long pants as shown in Fig. 1. We start with an initial pattern set that leads to about 30% stretch along the circumference of the legs. Since the seams are initially perpendicular to the direction of maximum stretch, they experience excessive traction forces. We then optimize the patterns using our seam-traction objective as well as the stretch objective in order to maintain the initial deformation. The optimization yields a pattern layout that leads to helical seams spiraling around the legs. The increased length and changed orientation leads to an overall improvement of 13% in traction force density. The optimized design thus reduces the risk of material failure while offering an aesthetically-interesting seam layout.

Pressure Objective. To evaluate the effectiveness of our pressure objective, we start with a simple example in which we optimize the patterns for a sphere such that the resulting pressure is as close as possible to $1000N/m^2$ everywhere. As can be seen in Fig. 5, the patterns change drastically during optimization and converge to elongated, winding shapes whose seams form a complex interlocking pattern on the 3D surface. Interestingly, this result is very similar to the one obtained by Skouras et al. [2014], who optimized patterns such that the inflated shape is as spherical as possible. It is not surprising then that optimizing for constant pressure yields patterns that result in an almost spherical shape.

Our second example for the pressure objective is a post-surgery compression mask consisting of two patterns. We set the admissible range of pressure to $1250 - 3000 N/m^2$, which is consistent with the target pressure of medical surgery masks. As shown in Fig. 6, the simulation result for the initial patterns exhibits excessive pressure for high-curvature regions such as the chin or the top of the head. Furthermore, there are many elements around the neck that exhibit negative pressure (shown in black), which occurs when cloth is stretching in concave regions. It should be noted that negative pressure is an artefact of our model and, rather than pulling on the body, the fabric would lift off the surface in reality. Nevertheless, it is an effective indicator for this problem and by penalizing negative pressure during optimization, we can prevent undesirable fabric lift-off. This effect can be observed in Fig. 6-right, where the optimized patterns achieve pressure values for sensitive areas within the desired range. While some elements with negative pressure remain in concave regions such as the temples or the hollows of the cheeks, their number is largely reduced.

Sliding Objective. We demonstrate the effectiveness of our sliding objective on a pair of long pants and four poses selected from a running sequence. We again prescribe a stretch target in the circumferential direction of the legs of 30% and set the friction coefficient to $\mu = 0.3$. As can be seen in Fig. 7, the pelvic area exhibits substantial tangential forces which would translate into unwelcome sliding during the motion. The optimized patterns lead to greatly reduced unbalanced tangential forces.

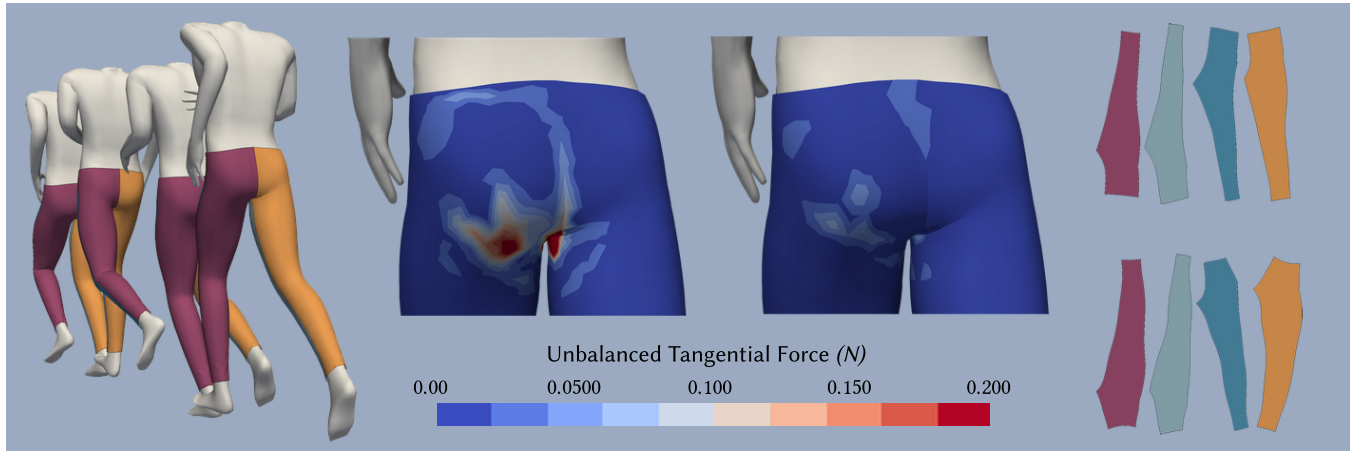


Fig. 7. Pattern optimization using our garment sliding objective. Left: the four input poses. Middle: tangential forces above the static friction limit in the pelvic area before (*top*) and after (*bottom*) optimization. Right: initial (*top*) and optimized (*bottom*) patterns.

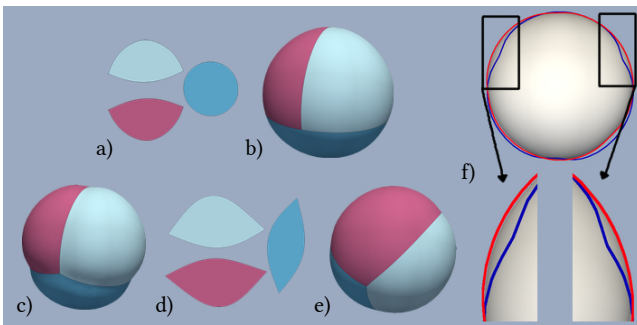


Fig. 8. Impact of seam stiffness. a) Patterns used in the simulation without seam stiffness and b) corresponding simulation result. c) Simulation result when using the patterns from a) with increased seam stiffness. d) Patterns optimized with seam stiffness and e) corresponding simulation result. f) Silhouette comparison between c) (*blue*) and e) (*red*).

6.2 Additional Evaluation

Impact of Seams. By accounting for seam stiffening in simulation, our method can anticipate the corresponding effects during pattern optimization. We demonstrate the impact of seams the example shown in Fig. 8. We simulate an initial pattern set (Fig. 8a) on a deformable sphere without seam stiffening, resulting in a shrunk version of the sphere (Fig. 8c). However, when the same patches are simulated again with added seam stiffness, the resulting shape exhibits clearly visible deformations around the seams (Fig. 8d). When optimizing the patterns with seam stiffness, using the initially deformed sphere as target (Fig. 8b), our method adjusts the patterns such that the resulting shape approximates well the target (Fig. 8e).

One central advantage offered by our optimization-driven approach over manual pattern design is that a given pattern layout can be automatically customized to a variety of body shapes. We demonstrate this ability by optimizing the patterns of wet-suit design, shown in Fig. 9, for four different body shapes using the same objective (30% target stretch) in all cases. Our method automatically

grades the patterns for each body shape such that the target stretch is maintained (Fig. 9-right).

Performance and Statistics. In all our results, we start from an initial guess obtained by scaling down the patterns computed with a geometric flattening method [Sheffer et al. 2005]. By scaling down patterns, we avoid slack elements at the start of the optimization. Each simulation is considered converged once the norm of the unbalanced forces falls below 10^{-6} . The optimization is considered converged once the norm of the objective gradient falls below 10^{-3} . We ran our examples on a machine with an Intel Core i7-5820k processor and 8GB of RAM. In terms of material parameters, we use a Young modulus of 24.78KPa and a Poisson's ratio of 0.49 for the body. For the cloth, we chose a thickness of 0.1mm and a Young modulus of 30MPa for the mask, 5.4MPa for the pants with a Poisson's ratio of 0.33 for all examples. Statistics for all experiments are listed in Table 1.

7 CONCLUSIONS, LIMITATIONS AND FUTURE WORK

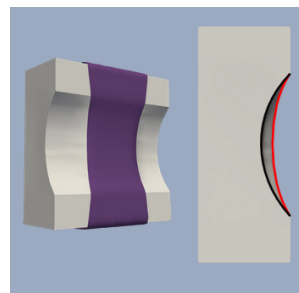


Fig. 10. Stretched cloth on a concave surface (*left*) results in pulling forces that can produce artifacts in the body (*right*).

We presented an optimization-driven approach to automatically generate patterns for skintight clothing. As the core of our method, we proposed a computational model that captures the mechanics of the clothing, the underlying body, and their mutual interaction within a unified approach. We furthermore described a set of design objectives that encode shape, comfort, and mechanical aspects of the garments. Our results indicate that our approach is able to reliably compute optimal patterns for



Fig. 9. Automatic pattern grading of a wet-suit design on a range of body shapes. *Left*: optimized patterns for the first body shape. *Middle*: four different body shapes shown in split view with pattern layout to the left and color-coded maximum stretch with corresponding directions to the right. *Right*: one of the patches optimized for each body shape.

Table 1. Summary of parameters and performance for all our experiments.

Model	# Patterns	# Remeshing steps	# iterations	Time per iteration [s]	Initial objective	Final objective
Cylinder tapered (Fig. 3b)	2	0	346	12.2	5433.58	106.952
Cylinder hourglass (Fig. 3c)	2	0	386	10.1	2241.66	222.638
Pants stretch (Fig. 1)	4	0	903	6.34	133.06	5.7029
Pants seam traction (Fig. 1)	4	1	4160	5.87	38.6195	28.4453
Pants shape (Fig. 4)	8	0	1408	19.2	66.9126	14.3992
Sphere pressure (Fig. 5)	3	5	2714	4.66	9547.41	205.544
Sphere shape (Fig. 8)	3	0	1001	22.3	22524.6	217.663
Mask pressure (Fig. 6)	2	0	849	6.40	55.4356	1.54963
Sliding pants (Fig. 7)	4	0	914	7.48	120.566	5.22695
Wetsuit regular (Fig. 9)	12	0	1629	5.84	130.225	19.7035
Wetsuit athletic (Fig. 9)	12	0	1735	5.57	139.744	21.1511
Wetsuit overweight (Fig. 9)	12	0	1353	6.60	177.552	25.8128
Wetsuit kid (Fig. 9)	12	0	1561	5.72	115.961	18.3544

a broad range of garments and body shapes, even when substantial design changes are required.

Our current approach has several limitations, most of which indicate promising directions for future work. Embedding the garment in the surface of the body simplifies both simulation and optimization. Nevertheless, it comes at the cost of introducing incorrect behaviour for concave surfaces: whereas real cloth will lift off the body when stretched over a concave region, in our model it generates traction forces that pull the body outwards as illustrated in the inset figure. While we can detect these situations and optimize patterns to avoid negative pressure, not all cases can be resolved in this way. In the future, it would be interesting to combine our approach with a conventional cloth model that is activated for regions in which the cloth separates from the body.

All our examples use a single isotropic cloth material for all patterns. Natural extensions include accounting for material anisotropy, and to combine patterns with different materials for shaping and reinforcement.

We use subdivision surfaces to convert the piece-wise linear boundary of the body mesh into a continuous surface. While the improved smoothness facilitates simulation and optimization, we do

currently not use the same representation for simulating the body. Increasing the resolution of the body mesh decreases the discrepancy between these representations, but a more elegant solution would be to use subdivision finite elements [Burkhart et al. 2010]. As a related limitation, the cloth mesh should have a higher resolution than the body mesh, since it could otherwise lead to body vertices not experiencing any coupling force. Finally, while our method allows for bounding the maximum stretch in a garment once worn, we do not take into account deformations that occur during dressing. Especially for tight-fitting garments made of stiffer fabrics, this question can have an important impact on the design. Integrating dressing simulation into the design process is an interesting direction, and the work of Clegg et al. [2015] seems a good starting point.

ACKNOWLEDGMENTS

We gratefully acknowledge the support of the Natural Sciences and Engineering Research Council of Canada (NSERC) from the Discovery Grants and Accelerator Awards programs (RGPIN-2014-05884 for TP and RGPIN-2017-05602 for BT). BT also acknowledges support from the Québec Research Council FRQNT.

REFERENCES

- David Baraff and Andrew Witkin. 1998. Large steps in cloth simulation. In *Proceedings of the 25th annual conference on Computer graphics and interactive techniques*. ACM, 43–54.
- David Baraff, Andrew Witkin, and Michael Kass. 2003. Untangling cloth. *ACM Transactions on Graphics (TOG)* 22, 3, 862–870.
- Aric Bartle, Alla Sheffer, Vladimir G. Kim, Danny M. Kaufman, Nicholas Vining, and Floraine Berthouzoz. 2016. Physics-driven Pattern Adjustment for Direct 3D Garment Editing. *ACM Trans. Graph.* 35, 4, Article 50, 11 pages.
- Miklós Bergou, Max Wardetzky, Stephen Robinson, Basile Audoly, and Eitan Grinspun. 2008. Discrete Elastic Rods. *ACM Transactions on Graphics* 27.
- Floraine Berthouzoz, Akash Garg, Danny M. Kaufman, Eitan Grinspun, and Maneesh Agrawala. 2013. Parsing Sewing Patterns into 3D Garments. *ACM Trans. Graph.* 32, 4, Article 85, 12 pages. <https://doi.org/10.1145/2461912.2461975>
- Javier Bonet and Richard D. Wood. 2008. *Nonlinear Continuum Mechanics for Finite Element Analysis* (2 ed.). Cambridge University Press. <https://doi.org/10.1017/CBO9780511755446>
- Robert Bridson, Ronald Fedkiw, and John Anderson. 2002. Robust treatment of collisions, contact and friction for cloth animation. In *ACM Transactions on Graphics (ToG)*, Vol. 21. ACM, 594–603.
- Remi Brouet, Alla Sheffer, Laurence Boissieux, and Marie-Paule Cani. 2012. Design Preserving Garment Transfer. *ACM Trans. Graph.* 31, 4, Article 36, 11 pages. <https://doi.org/10.1145/2185520.2185532>
- Daniel Burkhart, Bernd Hamann, and Georg Umlauf. 2010. Iso-geometric Finite Element Analysis Based on Catmull-Clark Subdivision Solids. *Computer Graphics Forum*.
- Xiaowu Chen, Bin Zhou, Fei-Xiang Lu, Lin Wang, Lang Bi, and Ping Tan. 2015. Garment modeling with a depth camera. *ACM Trans. Graph.* 34, 6, 203–1.
- Gabriel Cirio, Jorge Lopez-Moreno, David Miraut, and Miguel A Otaduy. 2014. Yarn-level simulation of woven cloth. *ACM Transactions on Graphics (TOG)* 33, 6, 207.
- Gabriel Cirio, Jorge Lopez-Moreno, and Miguel A Otaduy. 2015. Efficient simulation of knitted cloth using persistent contacts. In *Proceedings of the 14th ACM SIGGRAPH/Eurographics Symposium on Computer Animation*. ACM, 55–61.
- Alexander Clegg, Jie Tan, Greg Turk, and C. Karen Liu. 2015. Animating Human Dressing. *ACM Trans. Graph.* 34, 4, Article 116, 9 pages. <https://doi.org/10.1145/2766986>
- Philippe Decaudin, Dan Julius, Jamie Wither, Laurence Boissieux, Alla Sheffer, and Marie-Paule Cani. 2006. Virtual garments: A fully geometric approach for clothing design. In *Computer Graphics Forum*, Vol. 25. 625–634.
- Ye Fan, Joshua Litven, David IW Levin, and Dinesh K Pai. 2013. Eulerian-on-lagrangian simulation. *ACM Transactions on Graphics (TOG)* 32, 3, 22.
- Eitan Grinspun, Yotam Gingold, Jason Reisman, and Denis Zorin. 2006. Computing discrete shape operators on general meshes. *Computer Graphics Forum (Eurographics)* 25, 3, 547–556. <https://doi.org/10.1111/j.1467-8659.2006.00974.x>
- Peng Guan, Loretta Reiss, David A. Hirshberg, Alexander Weiss, and Michael J. Black. 2012. DRAPE: DRessing any PErson. *ACM Trans. Graph.* 31, 4, Article 35, 10 pages.
- David Harmon, Etienne Vouga, Breannan Smith, Rasmus Tamstorf, and Eitan Grinspun. 2009. Asynchronous contact mechanics. *ACM Transactions on Graphics (TOG)* 28, 3, 87.
- David Harmon, Etienne Vouga, Rasmus Tamstorf, and Eitan Grinspun. 2008. Robust treatment of simultaneous collisions. *ACM Transactions on Graphics (TOG)* 27, 3, 23.
- Dan Julius, Vladislav Kraevoy, and Alla Sheffer. 2005. D-charts: Quasi-developable mesh segmentation. In *Computer Graphics Forum*, Vol. 24. 581–590.
- Tsz-Ho Kwok, Yan-Qiu Zhang, Charlie C. L. Wang, Yong-Jin Liu, and Kai Tang. 2016. Styling Evolution for Tight-Fitting Garments. *IEEE Transactions on Visualization and Computer Graphics* 22, 5, 1580–1591. <http://dx.doi.org/10.1109/TVCG.2015.2446472>
- Bruno Lévy, Sylvain Petitjean, Nicolas Ray, and Jérôme Maillot. 2002. Least squares conformal maps for automatic texture atlas generation. In *ACM transactions on graphics (TOG)*, Vol. 21. ACM, 362–371.
- Duo Li, Shinjiro Sueda, Debanga R Neog, and Dinesh K Pai. 2013. Thin skin elastodynamics. *ACM Transactions on Graphics (TOG)* 32, 4, 49.
- Jie Li, Gilles Daviet, Rahul Narain, Florence Bertails-Descoubes, Matthew Overby, George E Brown, and Laurence Boissieux. 2018a. An implicit frictional contact solver for adaptive cloth simulation. *ACM Transactions on Graphics (TOG)* 37, 4 (2018), 52.
- Mínchen Li, Danny M. Kaufman, Vladimir G. Kim, Justin Solomon, and Alla Sheffer. 2018b. OptCuts: Joint Optimization of Surface Cuts and Parameterization. *ACM Trans. Graph.* 37, 6, Article 247, 13 pages. <https://doi.org/10.1145/3272127.3275042>
- Yuwei Meng, Charlie C. L. Wang, and Xiaogang Jin. 2012. Flexible Shape Control for Automatic Resizing of Apparel Products. *Comput. Aided Des.* 44, 1, 68–76.
- Mark Meyer, Mathieu Desbrun, Peter Schröder, and Alan H. Barr. 2003. Discrete Differential-Geometry Operators for Triangulated 2-Manifolds. In *Visualization and Mathematics III*, Hans-Christian Hege and Konrad Polthier (Eds.). Springer Berlin Heidelberg, 35–57.
- Yuki Mori and Takeo Igarashi. 2007. Plushie: An Interactive Design System for Plush Toys. *ACM Trans. Graph. (Proc. SIGGRAPH)*.
- Matthias Müller, Nuttapong Chentanez, Tae-Yong Kim, and Miles Macklin. 2015. Air meshes for robust collision handling. *ACM Transactions on Graphics (TOG)* 34, 4, 133.
- Jorge Nocedal and Stephen J. Wright. 2006. *Numerical Optimization* (second ed.). Springer, New York, NY, USA.
- Miguel A Otaduy, Rasmus Tamstorf, Denis Steinemann, and Markus Gross. 2009. Implicit contact handling for deformable objects. In *Computer Graphics Forum*, Vol. 28. 559–568.
- A Cengiz Öztireli, Gael Guennebaud, and Markus Gross. 2009. Feature preserving point set surfaces based on non-linear kernel regression. In *Computer Graphics Forum*, Vol. 28. 493–501.
- Simon Pabst, Sybille Krzywinski, Andrea Schenk, and Bernhard Thomaszewski. 2008. Seams and Bending in Cloth Simulation. In *Workshop in Virtual Reality Interactions and Physical Simulation "VRIPHYS"*, Francois Faure and Matthias Teschner (Eds.). The Eurographics Association. <https://doi.org/10.2312/PE/vriphys/vriphys08/031-038>
- Allen C Pipkin. 1986. The relaxed energy density for isotropic elastic membranes. *IMA journal of applied mathematics* 36, 1, 85–99.
- Roi Poranne, Marco Tarini, Sandro Huber, Daniele Panozzo, and Olga Sorkine-Hornung. 2017. Autocuts: Simultaneous Distortion and Cut Optimization for UV Mapping. *ACM Trans. Graph. (Proc. SIGGRAPH Asia)* 36, 6.
- Cody Robson, Ron Maharik, Alla Sheffer, and Nathan Carr. 2011. Context-aware garment modeling from sketches. *Computers & Graphics* 35, 3, 604–613.
- Pedro V Sander, John Snyder, Steven J Gortler, and Hugues Hoppe. 2001. Texture mapping progressive meshes. In *Proceedings of the 28th annual conference on Computer graphics and interactive techniques*. ACM, 409–416.
- Nicholas Sharp and Keenan Crane. 2018. Variational Surface Cutting. *ACM Trans. Graph.* 37, 4.
- Alla Sheffer, Bruno Lévy, Maxim Mogilnitsky, and Alexander Bogomyakov. 2005. ABF++: Fast and Robust Angle Based Flattening. *ACM Trans. Graph.* 24, 2 (April 2005). <https://doi.org/10.1145/1061347.1061354>
- Méline Skouras, Bernhard Thomaszewski, Peter Kaufmann, Akash Garg, Bernd Bickel, Eitan Grinspun, and Markus Gross. 2014. Designing Inflatable Structures. *ACM Trans. Graph. (Proc. SIGGRAPH)* 33, 4.
- Olga Sorkine, Daniel Cohen-Or, Rony Goldenthal, and Dani Lischinski. 2002. Bounded-distortion piecewise mesh parameterization. In *Proceedings of the conference on Visualization*. IEEE Computer Society, 355–362.
- Jos Stam. 1998. Evaluation of loop subdivision surfaces. In *SIGGRAPH*.
- Shinjiro Sueda, Garrett L Jones, David IW Levin, and Dinesh K Pai. 2011. Large-scale dynamic simulation of highly constrained strands. *ACM Transactions on Graphics (TOG)* 30, 4, 39.
- Emmanuel Turquin, Jamie Wither, Laurence Boissieux, Marie-Paule Cani, and John F Hughes. 2007. A sketch-based interface for clothing virtual characters. *IEEE Computer graphics and applications* 27, 1, 72–81.
- Nobuyuki Umetani, Danny M Kaufman, Takeo Igarashi, and Eitan Grinspun. 2011. Sensitive couture for interactive garment modeling and editing. *ACM Trans. Graph.* 30, 4, 90.
- Pascal Volino and Nadia Magnenat-Thalmann. 2006. *Resolving surface collisions through intersection contour minimization*. Vol. 25. ACM.
- Pascal Volino, Nadia Magnenat-Thalmann, and Francois Faure. 2009. A Simple Approach to Nonlinear Tensile Stiffness for Accurate Cloth Simulation. *ACM Trans. Graph.* 28, 4, Article 105, 16 pages.
- Charlie C. L. Wang and Kai Tang. 2008. Pattern computation for compression garment. In *Proceedings of the 2008 ACM symposium on Solid and physical modeling*. 203–211.
- Charlie C. L. Wang and Kai Tang. 2010. Pattern Computation for Compression Garment by a Physical/Geometric Approach. *Comput. Aided Des.* 42, 2, 78–86. <http://dx.doi.org/10.1016/j.cad.2009.02.018>
- Charlie C. L. Wang, Yu Wang, and Matthew M. F. Yuen. 2005. Design Automation for Customized Apparel Products. *Comput. Aided Des.* 37, 7, 675–691. <http://dx.doi.org/10.1016/j.cad.2004.08.007>
- Duo Wang, Xiangmin Jiao, Rebecca Conley, and James Glimm. 2013. On the curvature effect of thin membranes. *J. Comput. Phys.* 233, 449–463.
- Huamin Wang. 2018. Rule-free sewing pattern adjustment with precision and efficiency. *ACM Transactions on Graphics (TOG)* 37, 4, 53.
- Yu Wang, Alec Jacobson, Jernej Barbič, and Ladislav Kavan. 2015. Linear Subspace Design for Real-time Shape Deformation. *ACM Trans. Graph.* 34, 4, Article 57, 11 pages. <https://doi.org/10.1145/2766952>
- Nicholas J. Weidner, Kyle Piddington, David IW. Levin, and Shinjiro Sueda. 2018. Eulerian-on-Lagrangian Cloth Simulation. *ACM Transactions on Graphics* 37, 4, 50:1–50:11.
- Hitoshi Yamauchi, Stefan Gumhold, Rhaleb Zayer, and Hans-Peter Seidel. 2005. Mesh segmentation driven by Gaussian curvature. *The Visual Computer* 21, 8–10, 659–668.
- Jonas Zehnder, Stelian Coros, and Bernhard Thomaszewski. 2016. Designing Structurally-sound Ornamental Curve Networks. *ACM Trans. Graph.* 35, 4 (2016).
- Kun Zhou, John Snyder, Baining Guo, and Heung-Yeung Shum. 2004. Iso-charts: stretch-driven mesh parameterization using spectral analysis. In *Proceedings of the Eurographics/ACM SIGGRAPH symposium on Geometry processing*. 45–54.